



SAKARYA ÜNİVERSİTESİ

FEN BİLİMLERİ ENSTİTÜSÜ DERGİSİ

Sakarya University Journal of Science
SAUJS

e-ISSN 2147-835X Period Bimonthly Founded 1997 Publisher Sakarya University
<http://www.saujs.sakarya.edu.tr/>

Title: Hydrogen Generation from Methane on FeN₃ and FeN₄ Embedded Graphene Surface Using DFT Method with Grimme-D3 Dispersion Correction

Authors: Hilal KÜÇÜK

Received: 2021-06-29 00:00:00

Accepted: 2021-12-17 00:00:00

Article Type: Research Article

Volume: 26

Issue: 1

Month: February

Year: 2022

Pages: 62-73

How to cite

Hilal KÜÇÜK; (2022), Hydrogen Generation from Methane on FeN₃ and FeN₄ Embedded Graphene Surface Using DFT Method with Grimme-D3 Dispersion Correction. Sakarya University Journal of Science, 26(1), 62-73, DOI: 10.16984/saufenbilder.959390

Access link

<http://www.saujs.sakarya.edu.tr/tr/pub/issue/67934/959390>

New submission to SAUJS

<http://dergipark.gov.tr/journal/1115/submission/start>



Hydrogen Generation from Methane on FeN3 and FeN4 Embedded Graphene Surface Using DFT Method with Grimme-D3 Dispersion Correction

Hilal KÜÇÜK*¹

Abstract

In this article, the catalytic effect of Nx graphene embedded by Fe metal has been conducted for methane (CH_4) decomposition reaction using Density Functional Theory (DFT) calculations with Grimme-D3 dispersion correction. Recently, the catalytic activities of TMNx ($x=3\rightarrow 4$) graphene surfaces on chemical reactions have attracted a lot of attention. In particular, the activities of graphene surfaces can be increased by different numbers of doped nitrogen atoms on the graphene surface. For analyzing the adsorption mechanism, adsorption energy, Bader charge, charge density difference and the partial density of state have been calculated. CH_4 molecule is attached into FeN3 embedded graphene physically with higher adsorption energy (-0.41 eV) than that of FeN4 graphene. Their charge transfers from the molecule to the surface are quite small $0.0041e^-$ for FeN3 and $0.0003e^-$ for FeN4 graphene. The decomposition of methane has been calculated using the nudged elastic band method. There are the sequential four steps ($CH_x \rightarrow CH_{x-1} + H$, $x=4,3,2,1$). All reactions in these steps are endothermic. The activation energy of the first hydrogen production from methane ($CH_4 \rightarrow CH_3 + H$) on FeN3 surface is 0.39 eV while the barrier energy is 0.20 eV. However, the same reaction on FeN4 graphene has a quite high activation energy same as its barrier energy (1.84 eV), and its initial state switches directly to the final state without the transition state. The activation energies of most steps on FeN3 embedded graphene are much lower than that of FeN4 graphene surface. Therefore, dehydration reactions can occur with lower energy on FeN3 surface. This study can assist to discover a promising catalyst for methane dissociation through their finding.

Keywords: FeN3 embedded graphene; FeN4 embedded graphene; methane, CH4 decomposition; single-atom catalysis.

1. INTRODUCTION

Attention has been drawn to 2D nitrogen-carbon surfaces embedded by transition metals to improve catalyst knowledge. Xinrui Cao and colleagues

investigated the electric and magnetic behavior of TMN4 graphene surface (TM= Ti, V, Cr, Mn, Fe, Co, Ni, Cu) using DFT calculation [1]. According to their finding, lattice parameters of the surface can change their electronic and magnetic properties,

* Corresponding author: hilalkucuk@gazi.edu.tr

¹ Gazi University, Faculty of Science, Department of Physics,
 ORCID: <https://orcid.org/0000-0002-0777-1102>

and also the concentration of the TMN4 graphene can change its electronic properties from metallic to half-metallic or semiconducting characteristics. Putting different transition metals into the center of the surface causes different magnetic moments in the range from 0 to $4 \mu_B$. Xin et recently determined spin states modulation of TMN4 graphene surface has been determined by Xin et all. Their investigations are that TMN4 graphene sheets are energetically stable and have tunable magnetic properties [2]. K. Fajrial and colleagues studied the pyrolyzed Fe–N–C catalyst doped with boron to investigate the adsorption and decomposition of O_2 [3]. Many other valuable experimental and theoretical research has been extended to understand the oxygen reduction reaction using different approaches on TM-N-C catalyst for developing the fuel cell industry [4-10]. Gas adsorptions such as naphthenic acids [11], CO [12], CO_2 [13], NO , NO_2 , O_3 [14], and conversion such as dinitrogen to ammonia [15] have been studied on TM-N-C catalysts as well.

Through greenhouse gas (CH_4 , CO_2 , CH_3N , O_3 , water vapor), the temperature on Earth's surface is livable level. However, while the absence of greenhouse gas can cause its temperature would be lower than $-15^\circ C$, its extravagant increment makes the opposite effect; global warming [16]. Biogas, manure, rice farming, livestock farming, biomass burning, etc., pit gas, natural gas generate methane gas which increases this undesirable effect along with its rise [17, 18]. Additionally, if it exceeds its acceptable level, it might be responsible for Asphyxia and even death [19, 20]. To capture methane gas, many kinds of research have been made [21-24]. It is known that electronic and magnetic properties change after modification on graphene. Therefore, methane adsorption performances have been explored on graphene before and after modification by Gao's research group [25]. They tested graphene with single vacancy embedding Ni atom and double vacancy as well. According to their research, methane adsorption arises significantly after single vacancy defect and also including oxygen-containing functional groups. Another calculation of carbon

dioxide adsorption-assisted methane desorption on carbon surface showed that the addition of CO_2 to the environment makes methane is less stable on the surface compared with its single molecule adsorption [26].

Ammonia and methanol can be obtained from methane [27-30]. Additionally, hydrogen can be produced via methane decomposition without CO_x production for heating, electricity production, transportation, and industrial purposes and energy storage for portable devices. Hydrogen is a demanding energy source for clean energy. Although the usage of hydrogen energy in technology has been already started, its cost and performance should be improved using new catalysts [31-34]. To catalyze the reforming of methane, many studies have been performed such as methane decomposition on gold-nickel(111) surface [35], methane decomposition on 3d transition-metal clusters [36], and also many research about the reaction mechanism of CO_2 or H_2O activation for CH_4 reforming on various catalyst [37-42]. Ghanashyam Roy et al. worked on the dissociation of methane on Ni_4 cluster [43] and represented that the decomposition of CH_4 on the cluster is endothermic and not thermodynamically feasible at standard temperature and pressure. The other study of methane dissociation on Ni(111) with the presence of carbon showed that the increment of the activation barrier occurs along with the presence of carbon because the Ni-carbon surface repulses CH_x species[44]. Recently, the different aspect of dissociation mechanisms of methane on graphene sheets has been analyzed by Kun Li et al.[45] The finding was that almost all reaction energy barriers and reaction energies are higher on N-doped graphene compared with pristine graphene. The dissociation reactions from CH_4 to C_2H_2 can happen much easier on the vacancy graphene than that of N-doped graphene and pristine graphene.

The iron atom is the most preferable transition metal because the iron-based catalyst is well recognized and investigated. Fe-embedded metal $N_x(x=3,4)$ graphene can reduce the catalyst cost for

this process. In this study, methane decomposition for hydrogen production has been discussed on FeN3 embedded graphene compared with FeN4 graphene surface. The reaction mechanism of CH_x ($x = 1-4$) and the activation/reaction energies for each pathway were calculated to find the most promising catalysts for methane decomposition.

2. COMPUTATIONAL DETAIL

In density functional theory (DFT), all analyses were calculated using Quantum Espresso software package [46, 47]. To get rid of the core electrons and an extremely large number of plane waves, (PAW) pseudopotential were chosen with non-linear core correction and scalar relativistic [48, 49]. For all systems, the kinetic energy cutoff for charge density and potential was 520 Ry, and the kinetic energy cutoff for wave functions was 65 Ry. Gaussian smearing is 0.01 Ry for brillouin-zone. The first model of FeN3 moieties in graphene (FeN3-G) was created by single vacancy and then embedded by Fe transition metal surrounded by 3 nitrogen atoms using 5x5x1 cells with periodic boundary conditions with 50 atoms in Figure 1a. The second model of FeN4 moieties in graphene (FeN4-G) was built using double vacancy and then embedded by Fe transition metal surrounded by 4 nitrogen atoms using the same cells with periodic boundary conditions with 49 atoms in Figure 1b.

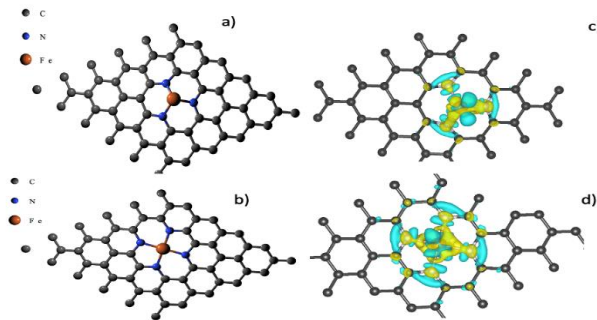


Figure 1 a) FeN3 graphene surface b) FeN4 graphene surface. C, Fe and N atoms represent gray, orange, and blue colors respectively. The charge density difference plot at iso-surfaces = $\pm 0.005 e/\text{\AA}^3$ c) for FeN3-G and d) for FeN4-G. The meaning of yellow color is the loss of electron density, and turquoise color is the gain of electron density.

There was an implementation of the term Grimme-D3 for Van der Waals and relatively weaker interactions corrections and also the spin polarization effect [50]. The gaussian spreading is 0.01 Ry for brillouin-zone integration. The lattice parameters were selected as $a=12.3 \text{ \AA}$ and $c=20 \text{ \AA}$ to have the lowest energy with 4x4x1 Monkhorst-Pack k-point mesh. The bond distance (d), magnetic moments after optimization are in Table 1. There is a good agreement with previous work by Cao's group[51]. Figures 1c-d are drawn as the charge density difference. These two plots show that electrons accumulate on the N atoms around the metal atom on both surfaces as losing charges from the metal.

The formation energy as

$$E_f = E_{surface} + n \cdot \mu_c - (E_{graphene} + m \cdot \mu_N + E_M) \quad (1)$$

where $E_{surface}$ and $E_{graphene}$ are respectively total energies of surface and pristine graphene.

Table 1 The bond distance (d), C_1 is on the right side of N atom on d_{N-C_1} and C_2 is on the left side. The second competitive results after slash on FeN4-G parameter belong to calculations taken by Cao's group[51]

Surface	d_{Fe-N} (\AA)	d_{N-C_1} (\AA)	d_{N-C_2} (\AA)	Magnetic Mom. (μ_B)	E_{form}
FeN3-G	1.862	1.376	1.376	3.0	-2.70
FeN4-G	1.89/1.91	1.37/1.38	1.39/1.38	2.0/1.97	-3.75

The number of carbon atoms removed from the pristine graphene is symbolized by n , and the number of nitrogen atoms on the surface systems is $m=3$ for FeN3 graphene and $m=4$ FeN4 graphene surface. μ_c and μ_N are the chemical potential of a single C atom and N respectively. E_{Fe} is the energy of the isolated Fe atom. The formation energies of these two surfaces are a negative value. This proves that both surfaces are stable.

The calculation of the adsorption energies (E_{ads}) of molecular structures on the surface as

$$E_{ads} = E_{surface+molecule} - E_{surface} - E_{molecule} \quad (2)$$

where $E_{\text{surface+molecule}}$ is the total energy of molecular structures on the surface. As E_{surface} is the total energy of the surface without molecule, E_{molecule} is the molecule energy in the gas phase. A release of energy during adsorption is demonstrated by the negative sign of adsorption energy. The transition state (TS) for structures is calculated by the nudged elastic band (NEB) method [52, 53]. The difference in energy between the final (E_{FS}) and the initial state (E_{IS}) gives the reaction barrier energy (E_R). The negative sign of reaction energy shows that reaction is exothermic while the endothermic process occurs in the positive value.

$$E_{act} = E_{TS} - E_{IS} \quad (3)$$

$$E_R = E_{FS} - E_{IS} \quad (4)$$

E_{act} is the activation and E_{TS} is the energy of TS. The electron transfer (Δq) is calculated by Bader charge analysis[54] as

$$\Delta q = q_{\text{surface+molecule}} - (q_{\text{surface}} + q_{\text{molecule}}) \quad (5)$$

The Bader charge of adsorbed molecule and surface is $q_{\text{surface+molecule}}$. Surface charge is q_{surface} and molecule charge is q_{molecule} . The negative sign or positive sign of Δq shows donating charge or gaining charge from the molecule.

Table 2 Some parameters for CH_4 on the graphene surfaces. d_{Fe-C} is the bond length between C atom on CH_4 and Fe on the surfaces. E_{ads} is the adsorption energy and d represents the length between two type atoms. d_{N-C_x} is the bond length between N and C atoms belonging to the surface as described above.

	E_{ads} (eV)	d_{Fe-N} (Å)	d_{N-C_1} (Å)	d_{N-C_2} (Å)	d_{Fe-C} (Å)	d_{C-H_1} (Å)	d_{C-H_2} (Å)	d_{C-H_3} (Å)	d_{C-H_4} (Å)	$\Delta q(CH_4)$ (e^-)
CH_4 in gas phase						1.096	1.096	1.096	1.096	
FeN3-G	-0.41	1.89	1.372	1.372	2.39	1.127	1.106	1.094	1.094	0.0041
FeN4-G	-0.17	1.89	1.39	1.37	3.25	1.096	1.097	1.096	1.096	0.0003

3. RESULT AND DISCUSSION:

3.1 Adsorption of CH_4 in FeN3 and FeN4 moieties in graphene

After the optimization of CH_4 on these surfaces, the most stable configurations are found as seen in Figure 3a for FeN3-G and Figure 4a for FeN4-G surfaces while CH_4 in the gas phase in Figure 2a. In Table 2, the bond lengths of $C-H_1$ and $C-H_2$ increase while the other hydrogen bond lengths are squeezed on FeN3-G surface. Also d_{Fe-N} is taller compared with its bare surface and d_{N-C_x} is getting smaller from 1.376Å to 1.372Å. The Bader charge exchange from molecule to FeN3-G is 0.0041 e^- as physical adsorption with the adsorption energy of -0.41 eV. Figure 3b illustrates the charge density difference plot. These all interactions can be viewed on the partial density of state (pDOS) Figure 3c as well. After methane adsorption(below plot of Figure3c) there is a big leap at the energy peak of H_1 and H_2 which are close to Fe atom and the energy peak of C between 7-8 eV interacting with Fe/3N atoms. However, they have very small effects in Figure 2b which is pDOS for methane in the gas phase. The sum of the energy peak of three nitrogen atoms where is near 0 on the bare surface (top plot) is getting lower after adding molecule.

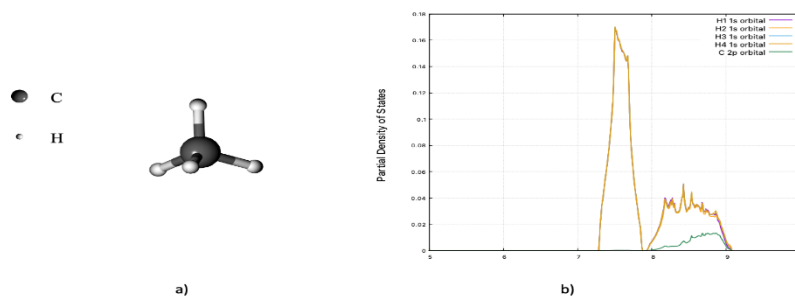


Figure 2 a) CH_4 on gas-phase b) Partial density of states (pDOS) of CH_4 in the gas phase. The energy of H_1 , H_2 , H_3 , H_4 and C atoms are represented by violet, orange, cyan, gold and green colors.

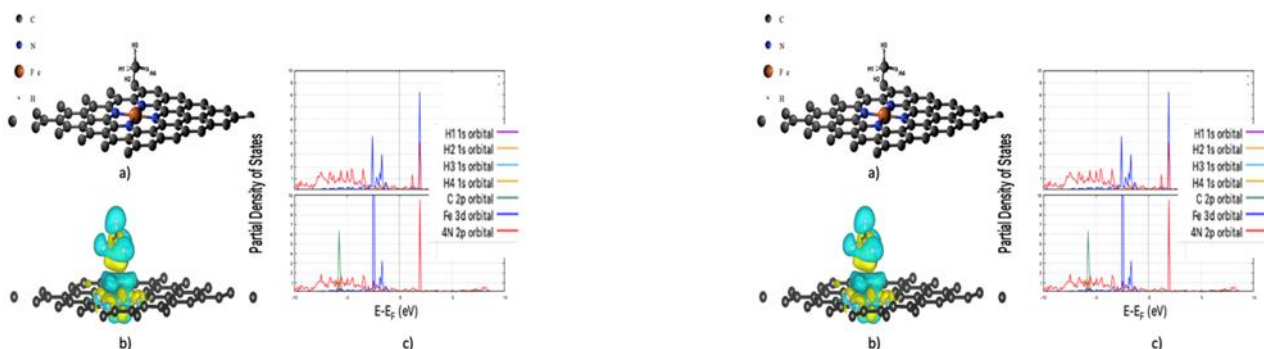


Figure 3 For the FeN3 graphene surface, a) CH_4 on the surface, b) The charge density difference plot at iso-surfaces = $\pm 0.001 \frac{e}{\text{\AA}^3}$, c) Partial density of states (pDOS) of CH_4 on the FeN3 graphene surface. The energy of H_1 , H_2 , H_3 , H_4 , C, Fe and the sum of three N atoms energies around Fe are represented by violet, orange, cyan, gold, green, blue and red colors. On this figure, the top plot represents pDOS on the bare surface and, the below plot is pDOS of molecule and surface after adsorption.

After adsorption, the molecule on the FeN4 surface remains almost the same except its elongated bond length of $C - H_2$. On the surface, there is a small increment on d_{N-C_1} while decrescent on d_{N-C_2} . This weak change can cause the weak charge exchange by $0.0003 e^-$ from molecule to FeN4 surface and physisorption with the adsorption energy of -0.17 eV. The charge density difference in Figure 4b shows that there is not a big charge transfer between molecule and surface. It is seen that there is not chemical interaction between molecule and surface.

Figure 4 For the FeN4 graphene surface, a) CH_4 on the surface, b) The charge density difference plot at iso-surfaces = $\pm 0.00012 \frac{e}{\text{\AA}^3}$, c) Partial density of states (pDOS) of CH_4 on the FeN4 graphene surface. The energy of H_1 , H_2 , H_3 , H_4 , C, Fe and the sum of four N atoms energies around Fe are represented by violet, orange, cyan, gold, green, blue and red colors. On this figure, the top plot represents pDOS on the bare surface and, the below plot is pDOS of molecule and surface after adsorption.

In the previous work[45], the methane adsorption in different sheets is similar to our result on FeN4-G. The interactions on different graphene sheets are physical with the adsorption energy of -0.13 eV on pristine graphene, the adsorption energy of -0.19 eV on N-doped graphene and the adsorption energy of -0.25 eV on vacancy graphene. However, methane is more stable on FeN3-G compared with the above surfaces.

Figure 4c is the partial density of state (pDOS) for FeN4-G. The small energy peak of H_2 is at near 6 eV and the peak of carbon atom increases

noticeably between 6-7 eV interacting with Fe/4N molecule after adsorption. The energy peak of Fe moves leftwards slightly with a big increment.

3.2 The decomposition of CH_4 on FeN3 graphene surface and FeN4 graphene surface

The decomposition steps with the initial, the transition and the final states are investigated as seen in Figure 5 for the FeN3 and Figure 6 for FeN4 surface. The various parameters are in Table 3 for CH_x ($x=1,2,3,4$) species for the adsorption reaction and Table 4 for the CH_x species co-adsorption reaction. Our strategy of the H cleavage is that the removed H atom from the molecule is put onto Fe or N atom on the surface and then NEB calculation is made for one of these two positions which have the most stable geometry. The reaction pathways and the calculation of E_{act}/E_R by NEB method as explained in the computational method section is shown in Table 5. The reaction energy diagram of the sequential pathway is shown in Figure 7. As explained before in section 2, the reaction is the endothermic process if E_r is the positive value. According to the barrier energies in the steps, all reactions are endothermic as the result of previous work on Ni_4 -cluster.

On FeN3 graphene surface, H_1 which has an elongated bond length from 1.096 Å to 1.217 Å in the adsorption geometry is broken off and settled on Fe atom with the distance of 1.54 Å with the co-adsorption energy of -4.70 eV. The activation energies and the reaction energy barrier of the first hydrogen production from CH_4 are respectively 0.39 eV and 0.20 eV on FeN3-G.

H_2 which has an elongated bond length with a small change by 0.001 Å on FeN4-G surface is removed from the molecule with $E_{act} = 1.84$ eV and the barrier energy is the same as activation energy. In this reaction, the initial state directly transfers into the final state without the transition state as seen in Figure 6a. . The same case happens in the second pathway ($CH_3 \rightarrow CH_2 + H$) on FeN3-G with high barrier energy, 2.63 eV. In the second step of the

hydrogen cleavage on FeN4-G, the C-H bond length increases from 1.086 Å to 1.098 Å. The distances between C and Fe atoms are 1.98 Å for FeN4-G after the adsorption and 1.73 Å after the co-adsorption. The broken H atom prefers to stay on the N atom with 1.034 Å of the distance. The reaction of $CH_3 \rightarrow CH_2 + H$ occurs with the activation energy of 2.91 eV and the barrier energy of 2.65 eV.

Table 3 The adsorption energy of CH_x and the bond length between atoms. The C-H bond length, d_{C-H} will be broken for CH_x decomposition.

	Species	E_{ads}	d_{C-H} (Å)		d_{Fe-C} (Å)
			Gas Phase	Adsorbed	
FeN3-G	CH_3	-3.04	1.086	1.102	1.96
FeN4-G		-2.58		1.098	1.98
FeN3-G	CH_2	-4.67	1.122	1.111	1.74
FeN4-G		-4.11		1.103	1.72
FeN3-G	CH	-5.75	1.137	1.103	1.62
FeN4-G		-4.60		1.116	1.63

In the third decomposition step, the distance of CH_2 molecule to the surface on Figure 5c (IS) for FeN3-G and Figure 6c (IS) for FeN4-G are respectively 1.74 Å and 1.72 Å. The adsorption/co-adsorption energies are -4.67/-7.90 eV for FeN3-G and -4.11/-6.78 eV for FeN4-G surface. On both surfaces, the broken H atoms are attached to N atoms with the distance of ~1.03 Å. The activation energies of the pathway on FeN3-G and FeN4-G are respectively 0.57 eV and 2.82 eV while the barrier energies are 2.09 eV and 2.65 eV. The activation energy of previous work on Ni_4 cluster[43] is quite higher with 1.28 eV than that of FeN3-G.

In the last step as seen in Figure 5d for FeN3-G and Figure 6d for FeN4-G, the CH adsorption energies are -5.75 eV and -4.60 eV respectively. C-H bonds on both surfaces are squeezed in the initial state, and carbon atoms are ~1.62 Å away from Fe atom on both surfaces. In the final state, H atom broken from CH molecule holds on N atoms with the distance of ~1.032 Å for both surfaces. The high

activation energies/barrier energies are observed on both surfaces, are 1.664/1.663 eV for FeN3-G and 1.80/1.25 for FeN4-G.

Table 4 The co-adsorption energy of $CH_x + H$ and the bond length of $Fe/N-H$ and $Fe-C$.

	Species	E_{ads}	$d_{Fe/N-H}$ (Å)	d_{Fe-C} (Å)
FeN3-G	$CH_3 + H$	-4.70	1.54	1.97
FeN4-G		-2.82	1.59	1.99
FeN3-G	$CH_2 + H$	-6.41	1.033	1.75
FeN4-G		-5.69	1.034	1.73
FeN3-G	$CH + H$	-7.90	1.029	1.64
FeN4-G		-6.78	1.03	1.65
FeN3-G	$C + H$	-8.01	1.032	1.54
FeN4-G		-7.26	1.031	1.55

Table 5 CH_4 decomposition pathways.

CH_4 Decomposition Pathways		FeN3 graphene E_{act}/E_r (eV)	FeN4 graphene E_{act}/E_r (eV)
TS1	$CH_4 \rightarrow CH_3 + H$	0.39/0.20	1.84/1.84
TS2	$CH_3 \rightarrow CH_2 + H$	2.63/2.63	2.91/2.65
TS3	$CH_2 \rightarrow CH + H$	0.57/2.09	2.82/2.65
TS4	$CH \rightarrow C + H$	1.664/1.663	1.80/1.25

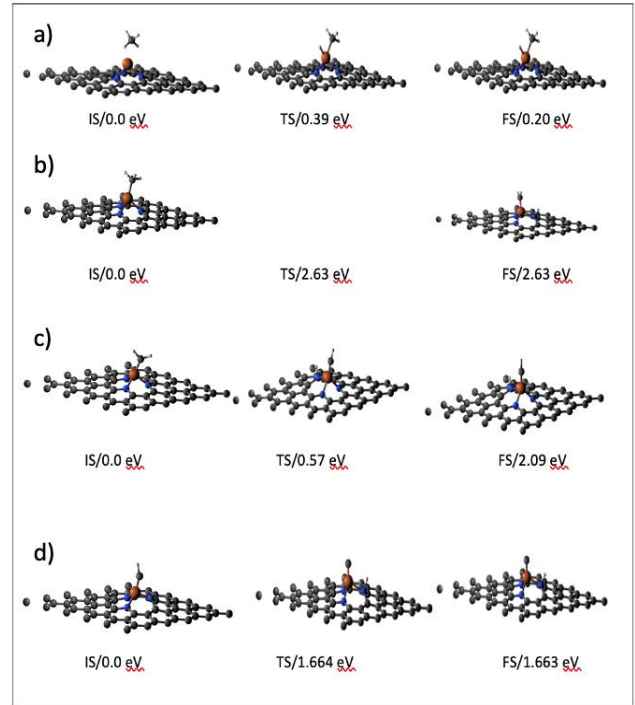


Figure 5 CH_x ($x=1 \rightarrow 4$) dehydrogenation generation pathway with the initial state (IS), the transition state (TS), the final state s(FS).

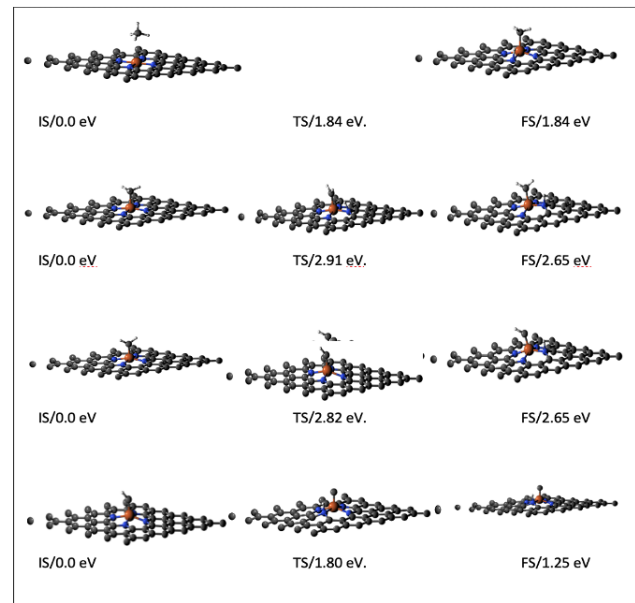


Figure 6 The CH_x ($x=1 \rightarrow 4$) dehydrogenation generation pathway with the initial state (IS), transition state (TS), the final state s(FS).

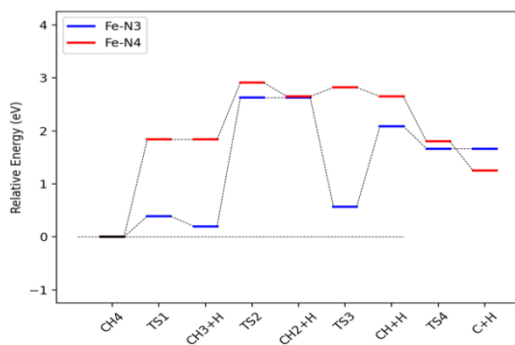


Figure 7 The reaction energy diagram of the sequential pathway. The reaction step is in Table-3 with related energy.

4. CONCLUSION

In this study, methane decomposition reaction mechanism on FeN3 embedded graphene and FeN4 embedded graphene were examined in detail using DFT density functional theory. On both surfaces, the physisorption interaction is observed for methane. In all steps, the most stable adsorption/co-adsorption geometries of CH_x ($x=1 \rightarrow 4$) were observed on FeN3-G surface with more interaction. When removed H atom from the molecule, the adsorption energy increased gradually, and the molecule was much closer than that of previous CH_x configuration. While H atom settled on Fe atom on the first H cleavage, it stayed on N atom on the other steps because molecule was quite close to Fe metal and H could not stay on Fe atom because of this closeness. For the first dehydrogenation step, the energy barrier required to break the C-H bond on both surfaces is quite low. This result shows that the surfaces on the C-H bond have high activation. In the second dehydrogenation step, the reaction step $CH_3 \rightarrow CH_2 + H$ is the rate-determining step of the overall reaction. Therefore, the highest energy barrier occurs at this step. Since the activation energy of 0.57 eV obtained on FeN3 in the next reaction step has a very low value, many expensive transition metals in the literature can be compared. In the last reaction step, the C-H bond is broken with an activation energy of 1.66 eV. The results obtained on the FeN3 graphene surface over the

entire reaction pathway are quite low and can be replaced with other costly transition metals. With this feature, FeN3 graphene has the potential to be a candidate material for hydrogen production from methane due to its low cost and high catalytic activity.

Acknowledgments

All computations calculations were made on TÜBİTAK ULAKBİM, High Performance and Grid Computing Center (TRUBA).

Funding

The author received no financial support for this work.

The Declaration of Conflict of Interest/ Common Interest

No conflict of interest or common interest has been declared by the author.

The Declaration of Ethics Committee Approval

This work does not require ethics committee permission or any special permission.

The Declaration of Research and Publication Ethics

The author of the paper declares that he complies with the scientific, ethical and quotation rules of SAUJS in all processes of the article and that she does not make any falsification on the data collected. In addition, she declares that Sakarya University Journal of Science and its editorial board have no responsibility for any ethical violations that may be encountered and that this study has not been evaluated in any academic publication environment other than Sakarya University Journal of Science.

REFERENCES

- [1] M.T. Baei, A. Soltani, and S. Hashemian, "Adsorption properties of hydrazine on pristine and Si-doped Al12N12 nano-cage,"

- Phosphorus, Sulfur, and Silicon and the Related Elements, vol. 191, no. 5, pp. 702-708, 2016.
- [2] X. Xin, et al., "Spin states modulation of Four-Nitrogen coordinated Transition-Metal (TMN₄) embedded graphene," *Applied Surface Science*, vol. 570, pp. 151126, 2021.
- [3] A.K. Fajrial et al., "First principles study of oxygen molecule interaction with the graphitic active sites of a boron-doped pyrolyzed Fe–N–C catalyst," *Physical Chemistry Chemical Physics*, vol. 19, no. 34, pp. 23497-23504, 2017.
- [4] C.W.B. Bezerra, et al., "A review of Fe–N/C and Co–N/C catalysts for the oxygen reduction reaction," *Electrochimica Acta*, vol. 53, no. 15, pp. 4937-4951, 2008.
- [5] B. Merzougui, et al., "A Pt-free catalyst for oxygen reduction reaction based on Fe–N multiwalled carbon nanotube composites," *Electrochimica Acta*, vol. 107, pp. 126-132, 2013.
- [6] G. Zhang, et al., "Is iron involved in the lack of stability of Fe/N/C electrocatalysts used to reduce oxygen at the cathode of PEM fuel cells?" *Nano Energy*, vol. 29, pp. 111-125, 2016.
- [7] S. Stariha, et al., "PGM-free Fe-N-C catalysts for oxygen reduction reaction: Catalyst layer design," *Journal of Power Sources*, vol. 326, pp. 43-49, 2016.
- [8] L. Yu, et al., "Oxygen reduction reaction mechanism on nitrogen-doped graphene: A density functional theory study," *Journal of Catalysis*, vol. 282 no. 1, pp. 183-190, 2011.
- [9] G. Wu, and P. Zelenay, "Nanostructured Nonprecious Metal Catalysts for Oxygen Reduction Reaction," *Accounts of Chemical Research*, vol. 46, no. 8, pp. 1878-1889, 2013.
- [10] Z. Lu, et al., "Novel catalytic activity for oxygen reduction reaction on MnN₄ embedded graphene: A dispersion-corrected density functional theory study," *Carbon*, vol. 84, pp. 500-508, 2015.
- [11] L. Ma and X. Chen, "Adsorption of naphthenic acids to the nitrogen-coordinated transition-metal embedded graphene: A DFT study," *Russian Journal of Physical Chemistry B*, vol. 10, no. 6, pp. 1027-1031, 2016.
- [12] Q.-K. Li, et al., "Cooperative spin transition of monodispersed FeN₃ sites within graphene induced by CO adsorption," *Journal of the American Chemical Society*, vol. 140, no. 45, pp. 15149-15152, 2018.
- [13] H. Bae, et al., "High-throughput screening of metal-porphyrin-like graphenes for selective capture of carbon dioxide," *Scientific reports*, vol. 6, no. 1, pp. 1-10, 2016.
- [14] C. Hu, et al., "Adsorption and sensing characteristics of air decomposed species onto pyridine-like PdN₃-doped CNT: a first-principles study," *Carbon Letters*, vol. 32, pp. 109-117, 2022.
- [15] X.-F. Li, et al., "Conversion of dinitrogen to ammonia by FeN₃-embedded graphene," *Journal of the American Chemical Society*, vol. 138, no. 28, pp. 8706-8709, 2016.
- [16] T.R. Karl, and K.E. Trenberth, "Modern Global Climate Change," *Science*, vol. 302, no. 5651, pp. 1719-1723, 2003.
- [17] L. Milich, "The role of methane in global warming: where might mitigation strategies be focused?" *Global Environmental Change*, vol. 9, no. 3, pp. 179-201, 1999.
- [18] A.R. Moss, J.-P. Jouany, and J. Newbold, "Methane production by ruminants: its contribution to global warming," in *Annales*

- de zootechnie. EDP Sciences, vol. 49, no.3, pp. 231-253, 2000.
- [19] R. Rossi, et al., "An unusual suicide: asphyxia by methane gas," *The American journal of forensic medicine and pathology*, vol. 34, no. 2, pp. 83-85, 2013.
- [20] M. Gasparik, et al., "First international inter-laboratory comparison of high-pressure CH₄, CO₂ and C₂H₆ sorption isotherms on carbonaceous shales," *International Journal of Coal Geology*, vol. 132, pp. 131-146, 2014.
- [21] K. Li, et al., "Adsorption of small hydrocarbons on pristine, N-doped and vacancy graphene by DFT study," *Applied Surface Science*, vol. 515, p. 146028, 2020.
- [22] W. Zhou, et al., "Hydrogen and methane adsorption in metal-organic frameworks: a high-pressure volumetric study," *The Journal of Physical Chemistry C*, vol. 111, no. 44, pp. 16131-16137, 2007.
- [23] W. Yuan, et al., "Experimental study and modelling of methane adsorption and diffusion in shale," *Fuel*, vol. 117, pp. 509-519, 2014.
- [24] K. Fan, et al., "Three stages of methane adsorption capacity affected by moisture content," *Fuel*, vol. 231, pp. 352-360, 2018.
- [25] X. Gao, et al., "Performance of intrinsic and modified graphene for the adsorption of H₂S and CH₄: a DFT study," *Nanomaterials*, vol. 10, no. 2, pp. 299, 2020.
- [26] H. Xu, et al., "CO₂ adsorption-assisted CH₄ desorption on carbon models of coal surface: A DFT study," *Applied Surface Science*, vol. 375, pp. 196-206, 2016.
- [27] A. Valera-Medina, et al., "Ammonia, Methane and Hydrogen for Gas Turbines," *Energy Procedia*, vol. 75, pp. 118-123, 2015.
- [28] X. Bai, et al., "Microwave catalytic synthesis of ammonia from methane and nitrogen," *Catalysis Science & Technology*, vol. 8, no. 24, pp. 6302-6305, 2018.
- [29] H.F. Abbas, and W.M.A. Wan Daud, "Hydrogen production by methane decomposition: A review," *International Journal of Hydrogen Energy*, vol. 35, no. 3, pp. 1160-1190, 2010.
- [30] A. Akça, "Conversion of methane to methanol on C-doped boron nitride: A DFT study," *Computational and Theoretical Chemistry*, vol. 1202, pp. 113291, 2021.
- [31] I. Staffell, et al., "The role of hydrogen and fuel cells in the global energy system," *Energy & Environmental Science*, vol. 12, no. 2, pp. 463-491, 2019.
- [32] H. Council, "Hydrogen scaling up: A sustainable pathway for the global energy transition," 2017.
- [33] E.S. Hanley, J.P. Deane, and B.P.Ó. Gallachóir, "The role of hydrogen in low carbon energy futures—A review of existing perspectives," *Renewable and Sustainable Energy Reviews*, vol. 82, pp. 3027-3045, 2018.
- [34] S. Dunn, "Hydrogen futures: toward a sustainable energy system," *International Journal of Hydrogen Energy*, vol. 27, no. 3, pp. 235-264, 2002.
- [35] H. Liu, et al., "A DFT theoretical study of CH₄ dissociation on gold-alloyed Ni (111) surface," *Journal of natural gas chemistry*, vol. 20, no. 6, pp. 611-617, 2011.
- [36] K.F. Andriani, J. Mucelini, and J.L.F. Da Silva, "Methane dehydrogenation on 3d 13-atom transition-metal clusters: A density functional theory investigation combined with Spearman rank correlation analysis," *Fuel*, vol. 275, pp. 117790, 2020.

- [37] S. Jiang, et al., "Insight into the reaction mechanism of CO₂ activation for CH₄ reforming over NiO-MgO: A combination of DRIFTS and DFT study," *Applied Surface Science*, vol. 416, pp. 59-68, 2017.
- [38] Y. Guo, J. Feng, and W. Li, "Effect of the Ni size on CH₄/CO₂ reforming over Ni/MgO catalyst: A DFT study," *Chinese Journal of Chemical Engineering*, vol. 25, no. 10, pp. 1442-1448, 2017.
- [39] Y.-P. Guo, W.-Y. Li, and J. Feng, "Reaction pathway of CH₄/CO₂ reforming over Ni₈/MgO (100)," *Surface Science*, vol. 660, pp. 22-30, 2017.
- [40] R. Ghanbari, R. Safaiee, and M. Golshan, "A dispersion-corrected DFT investigation of CH₄ adsorption by silver-decorated monolayer graphene in the presence of ambient oxygen molecules," *Applied Surface Science*, vol. 457, pp. 303-314, 2018.
- [41] MA. Lourenço, et al., "Interaction of CO₂ and CH₄ with functionalized periodic mesoporous phenylene-silica: Periodic DFT calculations and gas adsorption measurements," *The Journal of Physical Chemistry C*, vol. 120, no. 7, pp. 3863-3875, 2016.
- [42] A. Akça and İ.Ö. Alp, "The Dissociation Reaction of Methane on Ti-And Co-Embedded Graphene: A Dft Study," *Theory and Research in Science and Mathematics*, pp. 45-64, Gece kitablığı, ISBN. 978-625-7243-77-3, 2020
- [43] G. Roy, and A.P. Chattopadhyay, "Dissociation of methane on Ni₄ cluster-A DFT study," *Computational and Theoretical Chemistry*, vol. 1106, pp. 7-14, 2017.
- [44] J. Li, E. Croiset and L. Ricardez-Sandoval, "Effect of carbon on the Ni catalyzed methane cracking reaction: A DFT study," *Applied Surface Science*, vol. 311, pp. 435-442, 2014.
- [45] K. Li, et al., "Dissociation mechanisms of CH₄ on pristine, N-doped and vacancy graphene by DFT study," *Diamond and Related Materials*, vol. 114, p. 108323, 2021.
- [46] P. Giannozzi, et al., "QUANTUM ESPRESSO: a modular and open-source software project for quantum simulations of materials," *Journal of Physics: Condensed Matter*, vol. 21, no. 39, p. 395502, 2009.
- [47] P. Giannozzi, et al., "Advanced capabilities for materials modelling with Quantum ESPRESSO," *Journal of Physics: Condensed Matter*, vol. 29, no. 46, pp. 465901, 2017.
- [48] W. Kohn and L.J. Sham, "Self-Consistent Equations Including Exchange and Correlation Effects," *Physical Review*, vol. 140, no. 4A, pp. 1133-1138, 1965.
- [49] P.E. Blöchl, "Projector augmented-wave method," *Physical Review B*, vol. 50, no. 24, pp. 17953-17979, 1994.
- [50] S. Grimme, J. Antony, S. Ehrlich and H. Krieg, "A consistent and accurate ab initio parametrization of density functional dispersion correction (DFT-D) for the 94 elements H-Pu," *Journal of Chemical Physics*, vol. 132, p. 154104, 2010.
- [51] X. Cao, X.F. Li and W. Hu, "Tunable Electronic and Magnetic Properties of Graphene-Embedded Transition Metal-N₄ Complexes: Insight From First-Principles Calculations," *Chemistry—An Asian Journal*, vol. 13, no. 21, pp. 3239-3245, 2018.
- [52] G. Mills and H. Jónsson, "Quantum and thermal effects in H₂ dissociative adsorption: Evaluation of free energy barriers in multidimensional quantum systems," *Physical Review Letters*, vol. 72, no. 7, p. 1124, 1994.
- [53] G. Mills, H. Jónsson and G.K. Schenter, "Reversible work transition state theory:

application to dissociative adsorption of hydrogen,” *Surface Science*, vol. 324, no. 2-3, pp. 305-337, 1995.

- [54] G. Henkelman, A. Arnaldsson, and H. Jónsson, “A fast and robust algorithm for Bader decomposition of charge density,” *Computational Materials Science*, vol. 36, no. 3, pp. 354-360, 2006.